Stem Cell Reports

Article

Human induced pluripotent stem cell-derived atrial cardiomyocytes carrying an *SCN5A* mutation identify nitric oxide signaling as a mediator of atrial fibrillation

Liang Hong,[1,6,*] Meihong Zhang,[1,6] Olivia Thao Ly,[1] Hanna Chen,[1] Arvind Sridhar,[1] Erin Lambers,[1] Brandon Chalazan,[1] Seock-Won Youn,[1] Mark Maienschein-Cline,[2] Leonid Feferman,[2] Sang-Ging Ong,[1,3] Joseph C. Wu,[4] Jalees Rehman,[1,3] and Dawood Darbar[1,3,5,*]

[1]Division of Cardiology, Department of Medicine, Chicago, IL, USA
[2]Research Informatics Core, Research Resources Center, Chicago, IL, USA
[3]Department of Pharmacology, University of Illinois at Chicago, Chicago, IL, USA
[4]Stanford Cardiovascular Institute, Stanford University School of Medicine, Stanford, CA, USA
[5]Jesse Brown Veterans Administration Medical Center, Chicago, IL, USA
[6]These authors contributed equally
*Correspondence: hong2004@uic.edu (L.H.), darbar@uic.edu (D.D.)
https://doi.org/10.1016/j.stemcr.2021.04.019

SUMMARY

Mutations in *SCN5A*, encoding the cardiac sodium channel, are linked with familial atrial fibrillation (AF) but the underlying pathophysiologic mechanisms and implications for therapy remain unclear. To characterize the pathogenesis of AF-linked *SCN5A* mutations, we generated patient-specific induced pluripotent stem cell-derived atrial cardiomyocytes (iPSC-aCMs) from two kindreds carrying *SCN5A* mutations (E428K and N470K) and isogenic controls using CRISPR-Cas9 gene editing. We showed that mutant AF iPSC-aCMs exhibited spontaneous arrhythmogenic activity with beat-to-beat irregularity, prolonged action potential duration, and triggered-like beats. Single-cell recording revealed enhanced late sodium currents ($I_{Na,L}$) in AF iPSC-aCMs that were absent in a heterologous expression model. Gene expression profiling of AF iPSC-aCMs showed differential expression of the nitric oxide (NO)-mediated signaling pathway underlying enhanced $I_{Na,L}$. We showed that patient-specific AF iPSC-aCMs exhibited striking *in vitro* electrophysiological phenotype of AF-linked *SCN5A* mutations, and transcriptomic analyses supported that the NO signaling pathway modulated the $I_{Na,L}$ and triggered AF.

INTRODUCTION

Atrial fibrillation (AF), the most common cardiac arrhythmia in clinical practice, represents a major public health challenge. Currently over 33 million people worldwide suffer from AF and the burden of the arrhythmia is likely to rise as the population ages (Chugh et al., 2014). The AF epidemic places tremendous burden on healthcare costs in society with frequent hospitalizations and the associated morbidity and increased mortality (Friberg et al., 2003).

Over the past 15 years, positional cloning and next generation sequencing have identified AF-linked mutations in cardiac ion channels (Chen et al., 2003; Darbar et al., 2008; Enriquez et al., 2016; Ritchie et al., 2012), signaling molecules, and sarcomeric proteins (Gudbjartsson et al., 2017; Orr et al., 2016; Peng et al., 2017). Although genetic approaches to the mechanisms of AF have provided important insights into the underlying pathophysiology, direct impact of these discoveries to the bedside care of patients has been limited in part because *in vitro* methods to characterize mutations associated with AF fail to capture the full spectrum of functional changes (Darbar and Roden, 2013; Watanabe et al., 2011). Furthermore, cardiac

ion channels in transgenic murine models are species specific and may not precisely reproduce the human AF phenotype.

There is increasing interest in developing cellular models of disease that are genetically matched to specific patients using human induced pluripotent stem cells (iPSCs) (Itzhaki et al., 2011; Moretti et al., 2010). This approach has been used to generate large numbers of patient-specific iPSC lines and differentiate them into specific cardiac cell types, including atrial, nodal, and ventricular types (Devalla et al., 2015; Lee et al., 2017). Human iPSC-derived atrial (a) CMs have emerged as a new model to not only study AF mechanisms but also test pharmacological responses to antiarrhythmic drugs as they preserve the exact genetic context of the AF-linked mutations (Argenziano et al., 2018).

We previously identified *SCN5A* (encoding cardiac Na$_v$1.5 sodium channel) mutations associated with AF (Darbar et al., 2008). Here, we applied iPSC technology as well as a CRISPR/Cas9 (clustered regularly interspaced short palindromic repeats-associated 9) approach performing electrophysiological, pharmacological, and mechanistic analyses to explore the underlying mechanisms of AF-linked *SCN5A* mutations. We showed that

patient-specific AF iPSC-aCMs exhibited a striking *in vitro* electrophysiological phenotype of AF-linked *SCN5A* mutations, and transcriptomic analyses suggested that the nitric oxide (NO) signaling pathway modulated late sodium currents ($I_{Na,L}$) and triggered AF.

RESULTS

SCN5A familial AF kindreds

We enrolled a 62-year-old white man who underwent an atrio-ventricular (AV) node ablation and implantation of a single-chamber pacemaker for drug-refractory AF (Darbar et al., 2008). An electrocardiogram (EKG) from the proband showed ventricular pacing with underlying AF (Figure 1A). As the proband reported a family history, ascertainment of family members revealed familial AF in a three-generation kindred (Figure 1B). Sequencing *SCN5A* in the proband and affected members identified a rare non-synonymous coding region mutation (E428K). The heterozygous G→A point mutation conferred substitution of a conserved glutamic acid residue with a lysine residue of SCN5A channel that is highly conserved across vertebrate species (Figures 1C–1E).

We enrolled a 19-year-old African American man who presented with symptomatic persistent AF at 17 years of age. An EKG from the proband while on AV nodal blocking drugs showed AF with controlled ventricular rates (Figure S1A). The patient had a strong family history of AF, with both his mother and maternal grandmother developing AF at a relatively young age (Figure S1B). Sequencing SCN5A in the proband identified a rare non-synonymous coding region mutation (N470K) that was highly conserved across vertebrate species (Figures S1C and S1D).

Genotype-phenotype correlation

The *SCN5A*-E428K proband (I:1, Figure 1B) who presented with symptomatic AF at 52 years was initially treated with sotalol and then amiodarone. However, he underwent AV node ablation and pacemaker implantation because he developed persistent AF. The proband's daughter (II:2) developed AF when 48 years old but, despite sotalol treatment, she continued to experience symptoms and was eventually treated with rate control therapy. The proband's grandson (III:1) presented with symptomatic AF at 35 years of age and underwent successful pulmonary vein isolation (PVI). He remains asymptomatic on no medications. Table S1 describes the clinical characteristics of the familial AF kindreds.

The *SCN5A*-N470K proband (I:1) who presented with symptomatic AF at 17 years of age (Table S1) was initially treated with AV nodal blocking agents but then underwent a successful PVI. The proband's mother (II:2), who developed early-onset AF in the absence of underlying cardiac disease, was initially treated with sotalol but, with frequent recurrences, also underwent a successful PVI. The proband's maternal grandmother presented with minimally symptomatic AF at age 52 years and has successfully been treated with rate control therapy.

Generation of AF iPSCs

Human iPSCs were generated from the *SCN5A*-mutation probands and unaffected family members who do not carry the variant (control). Independent clones of each cell line were derived from peripheral blood mononuclear cells by Sendai virus-based reprogramming as previously described (Argenziano et al., 2018; Liang et al., 2016). Patient-specific iPSCs were maintained on human recombinant vitronectin-coated plates in mTesR1 Basal medium. The generated iPSCs cell lines expressed pluripotency markers OCT4 and SOX2 (Figure 1F).

Gene correction of AF iPSCs using CRISPR/Cas9

To validate the pathogenicity of the AF-linked variant *SCN5A*-E428K, we generated an isogenic-control line by targeted gene correction (GC). Using CRISPR-Cas9 and ribonucleoprotein (RNP) complex containing the GC sequence and homology arms as the repair template, we generated a GC-E428K iPSC line (Figure 2A) with positive clones and site-specific GC confirmed by genomic sequencing (Figure 2B). The GC-E428K iPSCs expressed the typical pluripotency markers including OCT4 and SOX2 (Figure 1F) and maintained a normal karyotype (Figure 2C).

Generation and characterization of iPSC-aCMs

The iPSCs cell lines were first differentiated into CMs using the monolayer-based method and a coated layer of extracellular matrix (ECM), and then a retinoic acid (RA)-based protocol was applied to differentiated cells into iPSC-aCMs as previously described (Argenziano et al., 2018). To analyze the specific types of CMs generated from RA-treated versus control cells, we first examined relative gene expression levels of atrial and ventricular CM markers in iPSC-derived CMs from AF119 family (Figure 1). Real-time qPCR revealed that RA-treated iPSC-CMs exhibited increased expression of atrial markers (NPPA, Kv1.5) and decreased expression of ventricular (MYL2, MYH7) markers (Figure S2). We then examined the percentage of cells expressing ventricular marker MYL2 and atrial markers Kv1.5 and MYL7 (Figure S3). Flow cytometry revealed a significant decrease in the percentage of cells expressing MYL2 in RA-treated cells compared with DMSO-treated cells (Figures S3A–S3B). We showed a significant increase in the percentage of cells expressing Kv1.5 in RA-treated cells compared with DMSO-treated cells (Figures S3C–S3F). We further examined the second atrial marker
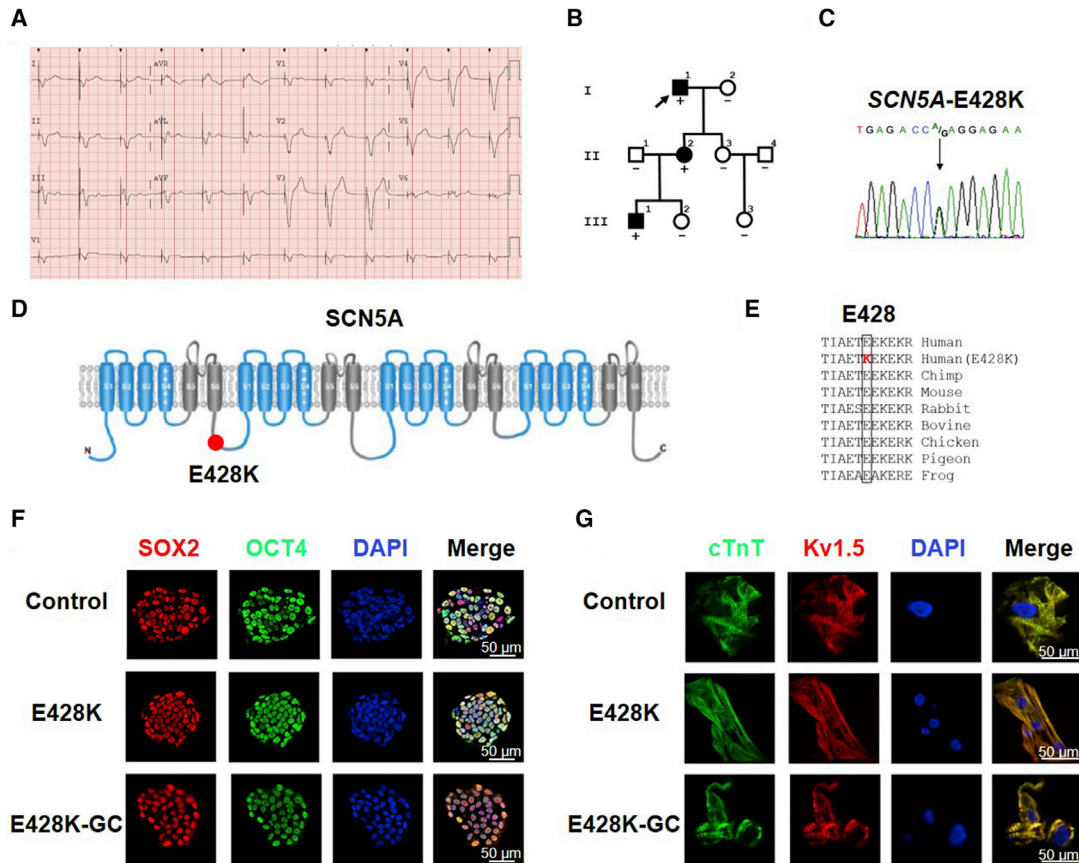
Figure 1. Generation and characterization of AF iPSC lines
(A) A 12-lead electrocardiogram (EKG) from the proband showing ventricular pacing with underlying AF.
(B) Pedigree of AF119 family that carries a rare *SCN5A*-E428K mutation. The presence (+) and absence (−) of the E428K mutation are indicated. The arrow denotes the proband. Squares and circles indicate male and female family members, respectively. Solid symbols indicate the presence of AF. Open symbols indicate unaffected members.
(C) Chromatogram showing heterozygous single-nucleotide change in the AF-linked *SCN5A*-E428K mutation at genomic coordinate Hg19 Chr3:38647498.
(D) Schematic representation of location of the mutation in the SCN5A sodium channel. The blue represents voltage-sensing domain, gray represents pore domain of the SCN5A channel, and E428K mutation is shown in red.
(E) *SCN5A* sequence alignment showing that the E428 is highly conserved across vertebrate species.
(F) Representative immunostaining of pluripotency markers SOX2 and OCT4 in iPSCs. The 4′,6-diamidino-2-phenylindole (DAPI) indicates the nucleus.
(G) Immunostaining showing the protein expression of pan-cardiomyocyte (CM) marker cTnT and atrial-specific marker $K_v 1.5$ in iPSC-aCMs. The DAPI staining indicates the nucleus.

MYL7 and ventricular marker MYL2, and confirmed that most RA-treated cells are differentiated into atrial cells (Figures S3G–S3J). Meanwhile, we showed a significant increase in the percentage of cells expressing Kv1.5 in RA-treated N470K iPSC-aCMs (Figures S1E–F).

Abnormal electrophysiological profiles in AF iPSC-aCMs
We first determined electrophysiological phenotype of iPSC-aCMs in a monolayer. Multi-electrode array (MEA) recordings were used to characterize cardiac field potential properties of control, E428K, E428K-GC iPSC-aCMs. The E428K atrial iPSC-CMs exhibited faster beating frequency, higher incidence of peak-to-peak interval variability (Figures 3A–3C, Table S2, Videos S1 and S2), and prolonged field potential duration (FPD) compared with controls (Figures 3D and 3E). Similar results were found in the second independently derived *SCN5A*-N470K iPSC-aCMs (Figures S4A–S4E, Table S2). We also showed that E428K AF iPSC-aCMs displayed spontaneous arrhythmogenic activity with beat-to-beat irregularity (Videos S1 and S2) suggestive of an AF-like phenotype (Zimetbaum, 2010).
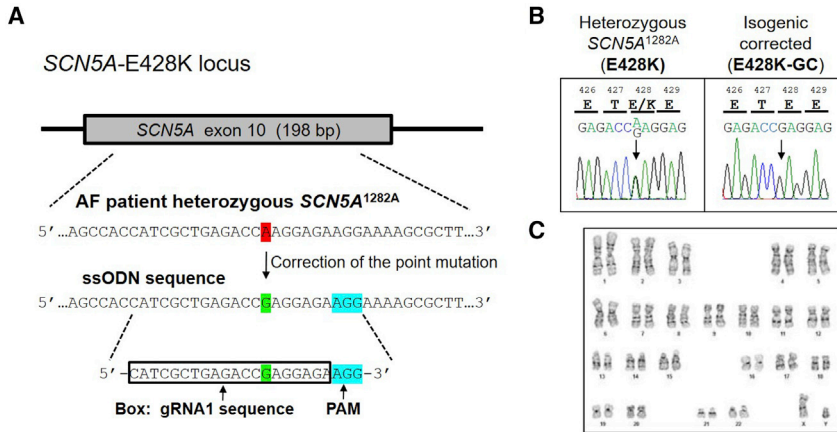
Figure 2. CRISPR/Cas9-mediated GC of the AF iPSC line carrying *SCN5A*-E428K mutation

(A) *SCN5A*-E428K locus for generation of GC-isogenic iPSCs with the *SCN5A*-1282A point mutation highlighted in red. The ssODN was used to correct the point mutation (highlighted in green) during directed repair of the Cas9-digested genome. Guide sequence (gRNA1 sequence) shown in small box was cloned into vector to express gRNA guiding Cas9 exonuclease to the targeted protospacer adjacent motif sequence (highlighted in cyan).

(B) Sequencing of the *SCN5A* gene in the isogenic-control iPSCs confirming E428K mutation correction.

(C) Karyotype analysis of the GC-iPSCs.

At the single-cell level, we characterized action potential (AP) profiles of the iPSC-aCMs cell lines, AP parameters including action potential duration at 90% repolarization (APD_{90}), maximal upstroke velocity (dV/dt_{max}), resting membrane potential (RMP), and the time between two adjacent peaks (interval). The E428K mutation iPSC-aCMs displayed shorter interval, faster upstroke, and prolonged APD compared with the control and E428K-GC cells (Figures 4A–4E, Table S3). Additionally, triggered-like beats were observed in the E428K mutant AF iPSC-aCMs (Figure 4A). In the *SCN5A*-N470K iPSC-aCMs, we also observed shorter intervals, faster dV/dtmax, and prolonged APD_{90} compared with the control cell line, with no significant differences in RMP between the cell lines (Figures S4F–S4K, Table S3).

We then investigated calcium transients in AF iPSC-aCMs because irregular APs associated with cardiac arrhythmias have been associated with abnormal calcium transients in CMs (Heijman et al., 2016; Heijman et al., 2012). The larger calcium transient amplitude exhibited by E428K mutant iPSC-aCMs may be due to differences in the spontaneous rate and sarcoplasmic reticulum calcium loading with the irregular calcium rhythm reflecting irregular AP firing (Figures S5A–S5C).

AF iPSC-aCMs displayed enhanced $I_{Na,L}$

We characterized sodium currents (I_{Na}) in iPSC-aCMs by a voltage clamp configuration, and showed that I_{Na} amplitude was not significantly changed in the E428K mutant AF iPSCs (Figures 4F and 4G). The AF iPSC-aCMs exhibited a minor hyperpolarization shift but there was no significant change. The $V_{1/2}$ was -42.6 ± 3.5 mV, -46.4 ± 3.6 mV, and -44.7 ± 3.0 mV in control, E428K, and E428K-GC iPSC-aCMs (Figure 4H). However, there was a marked increase in $I_{Na,L}$ in AF iPSC-aCMs but not in control and E429K-GC cells (Figures 4I and 4J). When we deter-mined the biophysical properties of the *SCN5A*-N470K iPSC-aCMs, it also showed increased $I_{Na,L}$ (Figures S4L–S4Q). The enhanced $I_{Na,L}$ may underlie the prolonged FPD, APD, and triggered-like beats (Figures 3, 4A–4E, and S4), consistent with a gain-of-function mechanism for the *SCN5A* mutation. We investigated SCN5A channel protein expression and found that there were no significant differences across the three cell lines (Figure S5D).

To determine if enhanced $I_{Na,L}$ is caused by E428K or N470K mutation-induced altered gating, we overexpressed the *SCN5A*-E428K mutation in human embryonic kidney (HEK) 293 cells. However, both the mutation and the wild-type (WT) SCN5A channels failed to exhibit persistent inward sodium currents (Figure S6). Enhanced $I_{Na,L}$, elicited in *SCN5A* mutation AF iPSC-aCMs but not in a heterologous expression system, suggested that channel dysfunction only becomes evident in the CM environment. One possible explanation is altered interactions with sodium channel partners, present in aCMs but absent in HEK293 cells.

Differential mRNA-level expression of NO signaling pathways in AF iPSC-aCMs

To explore potential partners interacting with the cardiac sodium channel, we performed transcriptomic analysis of the E428K control, E428K, and E428K GC iPSC-aCM lines. The major Gene Ontology (GO) categories identified by RNA sequencing and the most significantly modulated in the E428K iPSC-aCMs included cell differentiation, proliferation, and morphogenesis (Data S1). We selected the NO signaling pathway because studies have shown that $I_{Na,L}$ is enhanced in pathological states and regulated by cellular pathways including calmodulin kinase (CaMK), NO synthase (NOS), phosphoinositide 3-kinase (PI3K)-Akt, and protein kinase C (PKC) (Antzelevitch et al., 2014; Makielski, 2016). We hypothesized that mRNA-level
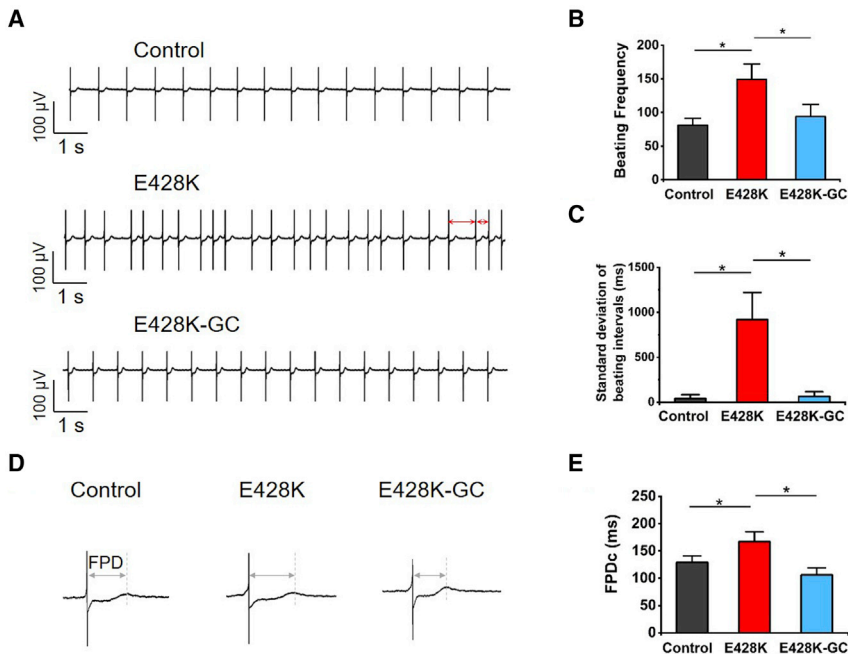
Figure 3. MEA recordings in iPSC-aCM monolayers

(A) Representative recordings from healthy control, E428K (middle), and E428-GC (bottom) iPSC-aCM monolayers. Red arrows show the peak-to-peak interval variability.

(B and C) The beating frequency (B) and incidence of peak-to-peak interval variability (C) in control, E428K, and E428-GC iPSC-aCMs. n = 8 independent experiments in each group, *p < 0.05.

(D and E) Representative MEA traces indicating FPDc; (D), and summary of FPDc values of control, E428K, and E428K-GC atrial iPSC-CMs (n = 8 independent experiments in each group (E)). *p < 0.05.

expression of signaling pathways involved in $I_{Na,L}$ post-translational modification in the AF iPSC-aCMs might differ from control cells.

We performed RNA sequencing to explore differential expressed genes (DEGs) of E428K AF iPSC-aCMs, and identified a total of 5,351 genes with 1,688 upregulated and 3,663 downregulated in the AF iPSC-aCMs. GO pathway analysis of DEGs revealed involvement of NO signaling pathways (Figure 5). We showed that genes such as *NOS1*, *NOS1* adapter protein (*NOS1AP*), NOS interacting protein (*NOSIP*), calmodulin 1 (*CALM1*), dimethylarginine dimethylaminohydrolase 1 (*DDAH1*), dihydrofolate reductase (*DHFR*), and lysophospholipase 1 (*LYPLA1*) involved in NO-mediated signal transduction and positive regulation of NO biosynthetic processes were upregulated in E428K AF iPSC-aCMs but rescued in E428K-GC cells (Figures S7A–S7G). Importantly, common genetic variants in genes encoding *NOS1* and *NOS1AP*, important for NO production in CMs, have been associated with arrhythmias (Ronchi et al., 2020; Tobin et al., 2008). We hypothesized that upregulation of *NOS1* and *NOS1AP* in the NO signaling pathway may underlie enhanced $I_{Na,L}$ in AF iPSC-aCMs. We validated the expression of *NOS1* and *NOS1AP* in E428K and control cells (Figures 6A–6C). Increased expression of *NOS1*, *NOS1AP*, and NO regulation of the cardiac sodium channel prompted us to determine if an NO blocker (N-ethylmaleimide) modulated $I_{Na,L}$ (Ahern et al., 2000). We showed a reduction in $I_{Na,L}$ in the AF iPSC-aCMs after treatment with N-ethylmaleimide (Figure 6D). We then determined Nav1.5 nitrosylation across the three cell lines

as nitrosylation of Nav1.5 increases $I_{Na,L}$ (Cheng et al., 2013). We showed that E428K AF iPSC-aCMs increased Nav1.5 nitrosylation which was rescued in E428K-GC cells (Figure 6E), indicating increased $I_{Na,L}$ in the mutant AF cell lines was associated with nitrosylation of Nav1.5.

We further assessed expression profiles of cardiac ion channels in E428K mutant iPSC-aCMs and showed differential mRNA-level expression (Figures S7H–S7N). Notably, upregulation of both ryanodine receptor type 2 (*RyR2*) and sarcoplasmic endoplasmic reticulum calcium ATPase 2 (*SERCA2*) may be linked with enhanced calcium handling in AF atrial iPSC-CM lines (Figures S5A and S7J–S7K).

Ranolazine rescued abnormal electrophysiological phenotype in AF iPSC-aCMs

We showed that 20 μM ranolazine, a $I_{Na,L}$ blocker, significantly reduced $I_{Na,L}$ in AF iPSC-aCMs (Figures 7A and 7B) and replicated these findings in the MEA recordings and calcium transient measurement showing that ranolazine reduced the peak-peak interval variability, beating frequency, and calcium transient amplitude of the AF iPSC-aCMs (Figures 7C–7H). Our data suggested that targeted inhibition of the $I_{Na,L}$ with ranolazine decreased the aberrant cellular electrophysiological phenotype of the AF iPSC-aCMs.

DISCUSSION

Using patient-specific iPSC-aCMs, we showed that an AF-linked SCN5A mutation recapitulated electrophysiological
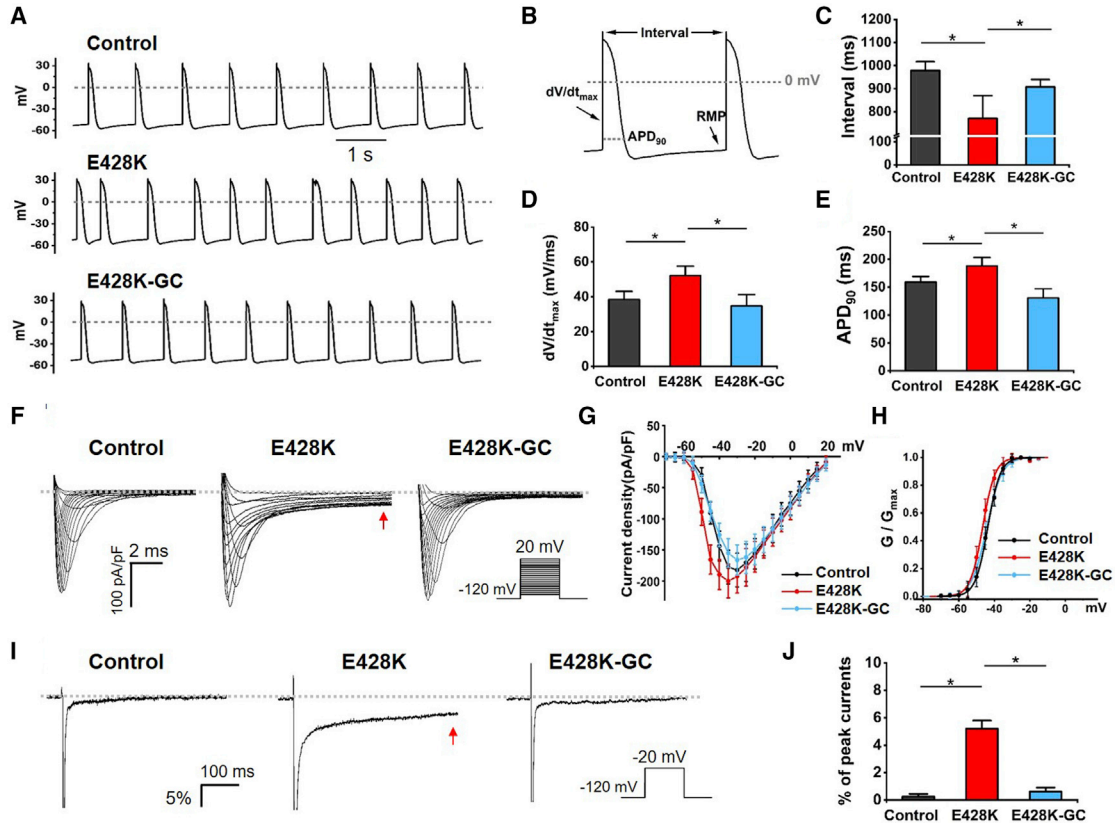
Figure 4. *SCN5A*-E428K iPSC-aCMs displayed abnormal AP profiles and enhanced $I_{Na,L}$

(A) Representative AP recordings from healthy control, E428K (middle), and E428-GC (bottom) iPSC-aCMs.

(B–E) (B) Atrial APs illustrating the measured parameters in iPSC-aCMs. (C–E) AP parameter comparison among control, E428K, and E428K-GC iPSC-aCMs, including (C) time between two adjacent peaks (interval); (D) maximal rate of rise (dV/dt_{max}); and (E) AP duration at 90% repolarization (APD_{90}), n = 20 single cells each group; for each group cell, the data were collected from six to eight independent cultures, *$p < 0.05$.

(F) Representative whole-cell sodium current traces recorded from control (left), E428K (middle), and E428K-GC iPSC-aCMs. Sodium currents were measured from a holding potential of −120 mV to test potentials ranging between −110 and +20 mV in 5-mV steps, followed by repolarization to −120 mV; dashed line represents 0pA.

(G) Current-voltage (I-V) relationship in the three groups of cells. Sodium current amplitude was normalized to the cell capacitance to obtain current density.

(H) Voltage dependence of sodium currents activation in the three groups of cells (n = 6 independent experiments each group); curves are Boltzmann fits of the data points.

(I) Representative $I_{Na,L}$ traces recorded in control (left), E428K (middle), and E428K-GC iPSC-aCMs; dashed line represents 0pA. Currents were activated by depolarization to −20 mV from a holding potential of −120 mV; red arrows show enhanced $I_{Na,L}$.

(J) E428K iPSC-aCMs displayed an enhanced $I_{Na,L}$ compared with control (n = 8 independent experiments each group); *$p < 0.05$.

phenotype with enhanced $I_{Na,L}$, APD prolongation, and triggered-like activity. RNA sequencing of AF iPSC-aCMs revealed differential expression of NO signaling pathways potentially underlying enhanced $I_{Na,L}$. Targeted inhibition of the $I_{Na,L}$ with ranolazine reduced arrhythmogenic activity and irregular beating in AF iPSC-aCMs. Our findings showed patient-specific AF iPSC-aCMs exhibited striking *in vitro* phenotypes of AF-linked SCN5A mutations and transcriptomic analyses suggested that the NO signaling pathway modulated $IN_{a,L}$ and triggered AF.

Modeling iPSC-aCMs

Patient-specific iPSC-aCMs are particularly suited to modeling AF-causing mutations as they elicit cell autonomous phenotypes. Despite variable penetrance of AF and modulation of clinical expression of ion channel mutations by co-morbidities such as hypertension—the so called two-hit hypothesis (Otway et al., 2007; Ritchie et al., 2012)—iPSC-based models may uncover distinct EP phenotypes and pharmacological responses at the cellular level. Such an approach not only enables us to examine
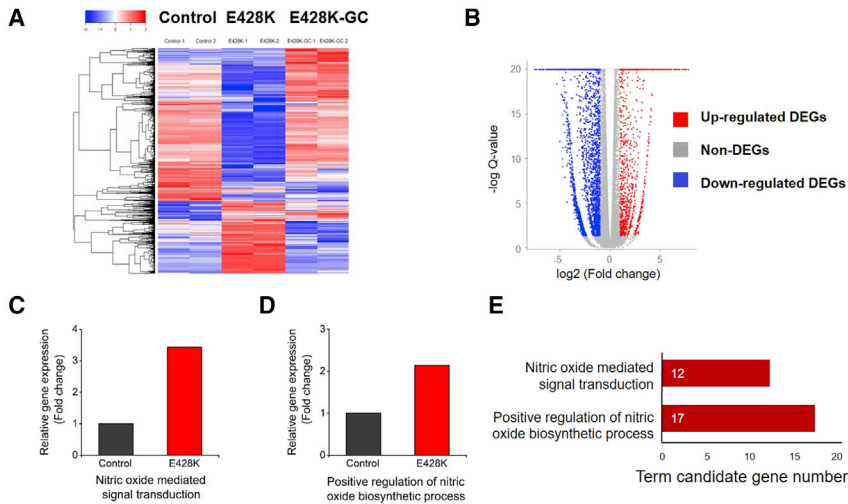
Figure 5. RNA sequencing analysis revealed differential transcriptome profile in mutant (AF) iPSC-aCMs

(A) Heatmap and hierarchical clustering of DEGs in the control, E428K, and E428K-GC iPSC-aCMs, n = 2 independent experiments for each group.

(B) Volcano plot with red points representing upregulated DEGs and blue points representing downregulated DEGs. Gray points represent non-DEGs.

(C–E) GO pathway analysis of DEGs revealed that some of them were significantly involved in NO-mediated signal transduction (C) and positive regulation of NO biosynthetic process (D). (E) Number of DEGs in both pathways.

the AF phenotype in different genetic backgrounds but also provides important insights into genotype-phenotype correlations, paving the way for a more personalized approach to AF therapy. Importantly, atrial embryonic stem cell CMs have been used to model pre-clinical testing of atrial-specific AADs, and the use of iPSC-aCMs can complement this model by deriving iPSCs from individual patients with AF.

A recent study modeled familial AF by generating iPSCs from two siblings and showed that the common genetic background of the patients induced ion channel remodeling and created a substrate for AF (Benzoni et al., 2020). However, this report used unrelated controls and failure to GC the AF-causing genes may have provided only limited insights into underlying pathophysiological mechanisms of familial AF. Here, we generated and characterized patient-specific atrial iPSCs from the AF proband, unaffected family member not harboring the *SCN5A* mutation, and the GC-isogenic control line. Our results not only confirmed the E428 variant as AF causing and uncovered a potential role for the NO signaling pathway in modulating $I_{Na,L}$ and triggered AF but also highlighted the importance of isogenic-control iPSC lines in modeling familial AF.

The $I_{Na,L}$ and AF

We showed that *SCN5A* mutant iPSC-aCMs displayed prolonged corrected FPD (FPDc) (Figure 3) and enhanced $I_{Na,L}$ (Figure 4), and ranolazine, a $I_{Na,L}$ blocker, reversed the AF-like phenotype (Figure 7) with reduced peak-peak interval variability, beating frequency, triggered-like beats, and calcium transient amplitude, supporting our hypothesis that increased $I_{Na,L}$ is arrhythmogenic and leads to AF. Support for our hypothesis comes from a study by Antzelevitch et al. (2014), who also reported that enhanced $I_{Na,L}$ is ar-

rhythmogenic and facilitates AF by prolonging the APD to increase the excitability of atrial myocytes and triggered activity. An increased $I_{Na,L}$ (often referred to as a gain of function in inherited arrhythmia syndromes) represents persistent depolarization of the atrial myocyte with prolongation of the APD, which corresponds to prolonged FPDc in our monolayer recording (Figure 3). Several diseases, including the long QT syndrome and dilated cardiomyopathy, have been associated with mutations in *SCN5A*, and a number of reports have linked *SCN5A* gain-of-function mutations and AF (Li et al., 2009; Lieve et al., 2017; Savio-Galimberti and Darbar, 2014). Although the mechanisms whereby some mutations produce AF and others generate ventricular phenotypes like long QT syndrome remains unclear, a possible explanation for the phenotypic variability in sodium channel-linked disease may be related to chamber- or disease-specific interactions between the channel and its partners (Savio-Galimberti and Darbar, 2014).

Notably, both mutations failed to increase the $I_{Na,L}$ when expressed in HEK293 cells (Figure S6), suggesting that sodium channel dysfunction only becomes evident in the milieu of atrial CMs and potentially altered expression of cellular signaling pathways such as NO linked with $I_{Na,L}$ in AF. One possible explanation is altered interactions with sodium channel partners, present in atrial CMs but absent in HEK293 cells. While we recorded irregular beats with abnormal AP shape that were suggestive of afterdepolarization-like triggered beats as reported by Liang et al. (2016) in iPSCs, the possibility that the beats may represent abnormal automaticity should be considered. We showed that *SCN5A*-E428K iPSC-aCMs displayed prolonged FPDc (Figure 3) and enhanced $I_{Na,L}$ (Figure 4), and ranolazine, a $I_{Na,L}$ blocker, reversed the AF-like phenotype (Figure 7) with reduced peak-peak interval variability, beating
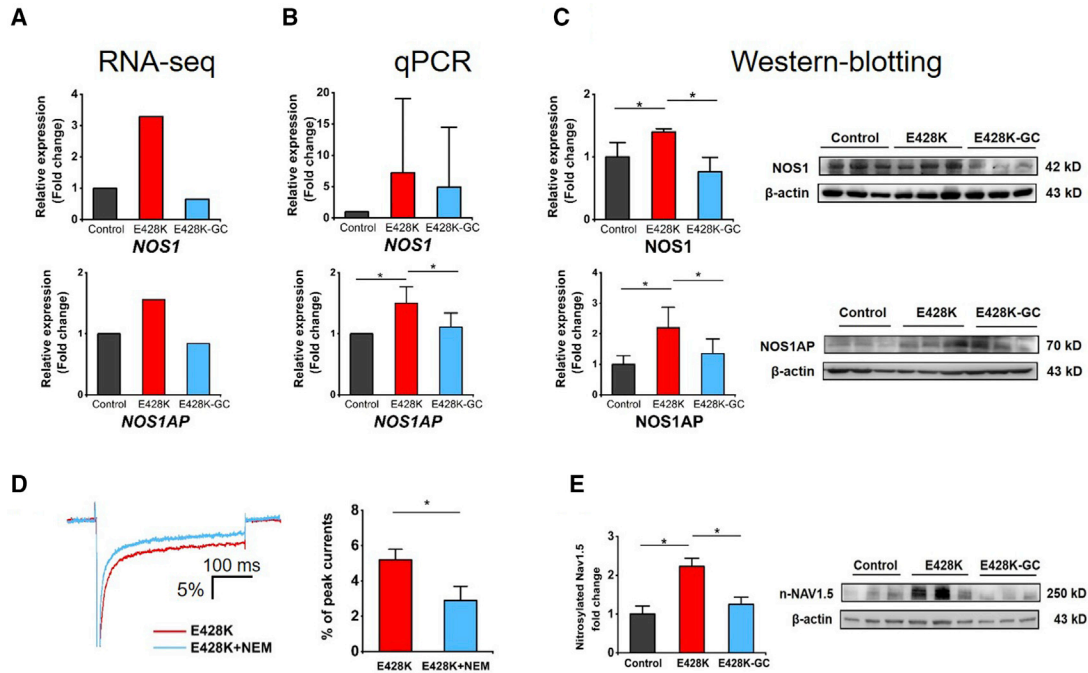
Figure 6. Abnormal expression of NOS proteins associated with dysfunction of *SCN5A*-E428K AF iPSC-aCMs

(A and B) Relative gene expression of *NOS1* (A) and *NOS1AP* (B) in control, E428K, and E428K-GC iPSC-aCMs from qPCR (n = 3 independent experiments for qPCR; *p < 0.05).

(C) Expression of *NOS1* proteins in iPSC-aCMs. (Left) Normalized expression of *NOS1* among the three iPSC-CMs (n = 6 independent experiments for each group; *p < 0.05). (Right) Representative western blot bands; β-actin is used for the loading control.

(D) N-ethylmaleimide (5 mM) inhibited $I_{Na,L}$ in the E428K AF iPSC-aCMs. The $I_{Na,L}$ was measured and normalized to peak current (n = 6 independent experiments, *p < 0.05).

(E) Enhanced nitrosylation of sodium channel Nav1.5 in E428K AF iPSC-aCMs. (Left) Relative ratio between nitrosylated Nav1.5 and total Nav1.5 in control, E428K, and E428K-GC iPSC-aCMs (n = 3 independent experiments for each group; *p < 0.05). (Right) Representative nitrosylation of Nav1.5 with β-actin as the loading control.

frequency, and calcium transient amplitude, supporting our hypothesis that the irregular beats represented afterdepolarization triggered-like beats.

The signaling pathways regulating the $I_{Na,L}$ are complex and include calcium/ CaMK, NOS, PKC, PI3K-Akt, and other signaling kinases (Makielski, 2016). One study showed that CaMKIIδ phosphorylated the cardiac sodium channel and enhanced $I_{Na,L}$ (Wagner et al., 2006), with another reporting that NO enhanced $I_{Na,L}$ under pathophysiological conditions (Ahern et al., 2000). It is also important to note that the *SCN5A*-E428K mutation is localized to the interdomain linker between domains 1 and 2. As activation of CaMKII is dependent on the interaction with calcium-calmodulin (CaM) at the inter domain linker region of Nav1.5, it is possible that the E428K mutation leads to increased CaMKII phosphorylation of the cardiac sodium channel and enhanced $I_{Na,L}$ (Hashambhoy et al., 2011).

Using human iPSC-aCMs, we showed for the first time that enhanced $I_{Na,L}$ associated with an AF-linked SCN5A

mutation is in part modulated by the NO signaling pathway. RNA sequencing showed that *NOS1* and *NOS1AP* were both upregulated in AF iPSC-aCMs and $I_{Na,L}$ was reduced by the NO inhibitor in aCMs. Collectively, our data suggest that that NO signaling plays an important role in modulating SCN5A and AF pathogenesis. While the precise mechanism(s) by which an *SCN5A* mutation modulates the NO signaling pathway remains unclear, one possibility is that the E428K variant alters the transcriptional regulation of NO genes. This is supported by our RNA sequence data (Figure S7) and studies showing that *SCN5A* is not only a regulator of gene transcriptional networks controlling cancer invasion (House et al., 2010) but also gene expression in neuronal and skeletal muscle cells (Tolon et al., 1996; Juretic et al., 2007).

Targeted medicine and clinical implications

Despite recent advances in catheter-based therapies, symptomatic AF is often treated with antiarrhythmic drugs (January et al., 2014). However, ~50% of patients
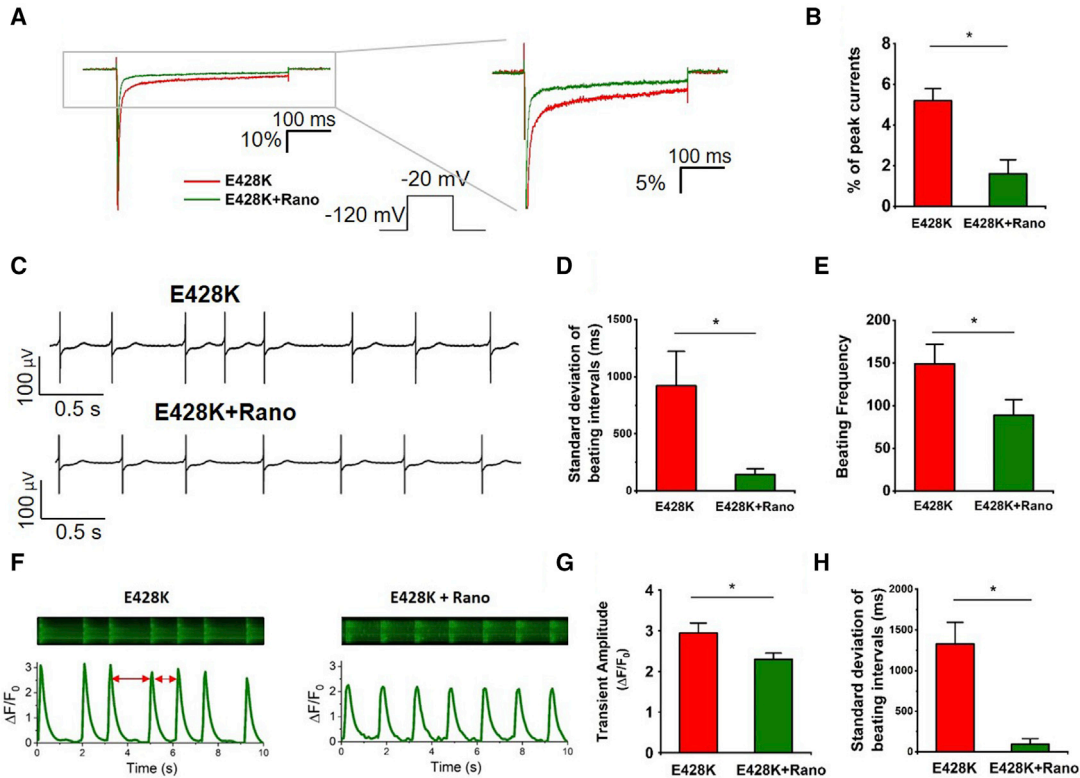
Figure 7. Effects of ranolazine (Rano) on *SCN5A*-E428K iPSC-aCMs

(A and B) Rano (20 μM) inhibited $I_{Na,L}$ in the E428K iPSC-aCMs. The $I_{Na,L}$ was measured and normalized to peak current (n = 6 independent experiments for E428K + Rano, n = 8 independent experiments for E428K).

(C–E) MEA recordings (C) indicated that Rano suppressed peak-peak interval variability (D) and beating frequency (E) in the E428K iPSC-aCM monolayers (n = 6 independent experiments for E428K + Rano, n = 8 independent experiments for E428K).

(F–H) Rano reduced abnormal calcium handling in E428K iPSC-CMs. Representative tracings of spontaneous calcium transients from E428K iPSC-CMs and those treated with 20 μM Rano; red arrows show the peak-to-peak interval variability (F). The calcium transient amplitude (G) and peak-to-peak interval variability (H) were decreased by 20 μM Rano treatment (n = 5 independent experiments for each group). *p < 0.05.

experienced symptomatic recurrence of AF within 6 months of starting membrane-active drugs (Darghosian et al., 2015). The limited pharmacological success of antiarrhythmic therapy for AF is due in part to the heterogeneity of the underlying substrate and failure to target therapy in individual patients (Darbar and Roden, 2013; Watanabe et al., 2011). Therefore, an *in vivo* modeling system that assesses response to targeted therapy would be a major advancement.

One potential implication of our findings is the development of mechanism-based therapies for AF. In our kindred family, members with AF carrying the *SCN5A* mutation did not respond to non-mechanism-based antiarrhythmic therapy. However, based on our findings using patient-specific iPSC-aCMs, it is plausible that a mechanism-based therapy such as the FDA-approved drug ranolazine may be more efficacious as it specifically blocks the $I_{Na,L}$ (Gupta et al., 2015; Polytarchou and Manolis, 2015). Furthermore,

some antiarrhythmic drugs are associated with serious toxicities, including drug-induced long QT syndrome, highlighting the importance of screening platforms for precision medicine. Modeling AF with patient-specific iPSC-aCMs has important implications for drug screening and drug discovery as well as enabling individualized assessments of efficacy and safety that guide clinicians toward personalizing therapy even before administering them to patients (Barichello et al., 2018).

Limitations

The predictive power of iPSC-CMs to serve as a platform for patient-specific studies may be limited by their immaturity compared with adult CMs, and it is possible that the electrophysiological phenotype of iPSC-aCMs does not fully recapitulate that of human adult atrial CMs. Recently, paracrine factors, including triiodothyronine, insulin-like growth factor-1, and dexamethasone, have been shown

to enhance ventricular iPSC-CM maturity ([Birket et al., 2015](); [Herron et al., 2016]()). However, less is known about the maturity of iPSC-aCMs and how paracrine factors or extracellular matrix influence their maturity; further studies are required to address these uncertainties. Another limitation of the current study is that even though we showed that upregulated NO signaling may underlie enhanced $I_{Na,L}$ in the AF E428K iPSC-aCMs, precisely how the mutation alters NO pathway gene expression remains unclear. This is an important question with broad implications and may reveal mechanistic insights into how ion channel activity modulates gene expression.

In summary, our findings showed that patient-specific iPSC-aCMs exhibited a striking electrophysiological phenotype of an AF-linked mutation that produced minimal changes *in vitro*, and suggested a link between enhanced $I_{Na,L}$, transcriptional regulation of NO signaling, and triggered AF. These findings not only provide insights into underlying cellular mechanisms of AF-linked mutations but also highlight potential mechanism-based therapies for this common arrhythmia.

EXPERIMENTAL PROCEDURES

Familial AF kindred

We enrolled two three-generation families with familial AF in a clinical-DNA biorepository. At enrollment, we asked all patients to complete a detailed medical and drug history and a symptom questionnaire and perform detailed phenotyping of probands and family members as previously described. We used the Vanderbilt University Medical Center and University of Illinois at Chicago (UIC) Institutional Review Board-approved protocol to enroll participants following informed written consent. Whole blood was collected for genomic DNA extraction and analysis from the proband and family members that consented to participate in the registry. Mutation screening of the PCR-amplified exons was performed by direct sequencing using the National Heart, Lung, and Blood Institute-supported Resequencing and Genotyping Service as previously described. All variants were validated by re-sequencing an independent PCR-generated amplicon from the subject.

Generation of iPSC lines

The iPSC lines were generated as previously described ([Argenziano et al., 2018]()). Three independent clones of each cell line were derived from peripheral blood by Sendai virus-based reprogramming. Human iPSCs were maintained on human recombinant vitronectin-coated plates in mTesR1 Basal medium (Gibco). The iPSCs were differentiated into iPSC-aCMs as we previously described ([Argenziano et al., 2018]()). Briefly, we treated cells with 1 μM RA for 5 days with media changes every other day, and a low-glucose metabolic selection step was then used to enrich CM culture. Human iPSC-aCMs showed typical expression of cardiac-specific marker cardiac troponin-T (cTnT), and atrial-specific marker Kv1.5.

GC of AF atrial iPSCs using CRISPR-Cas9

We edited iPSCs heterozygous for *SCN5A* p.E428K using CRISPR-Cas9. Briefly, we designed allele-specific guide (g) RNAs (5′-CATCGCTGAGACCAAGGAGA-3′) using the CRISPR program to target exon 10 containing the mutant allele. The iPSCs were treated with 10uM Y-27632 for an hour pre-electroporation, and then dissociated into single cells and electroporated with an RNP complex of Cas9 and sequence-guided (sg)RNA along with single-stranded oligodeoxynucleotides (ssODN) containing the WT template using the Neon Transfection System (Invitrogen). Immediately after electroporation, cells were transferred into one well of a Matrigel-coated 24-well plate containing 500 μL of mTesR with 10 μM Y-27632. After expansion for several days, we used half the cells to analyze editing efficiency with next-generation sequencing. Upon confirming editing efficiency, we then manually sorted 96 individual cells to establish single-cell colonies. A total of 21 edited clones were selected for expansion and verification of GC by sequencing. In addition to edited clones, we selected two unedited clones that were exposed to the genome-editing pipeline but remained unmodified.

Karyotype analysis

Karyotype analysis was performed by the Cytogenetics laboratory at WiCell Research Institute Inc. Cells were harvested and chromosomes were analyzed using the giemsa trypsin wright (GTW) banding method. Twenty metaphase cells were analyzed, all of which were concluded to have a normal karyotype (46, XY).

RNA sequencing

We extracted RNA with Maxwell RSC simplyRNA Cells Kit (Promega AS1390) based on manufacturer's instructions. RNA samples were normalized to 250 ng, and library prep was carried out using the Universal Plus mRNA-Seq kit (NuGen 0520-A01) as written in the product manual (NuGen M01485 v5). In brief, RNA underwent poly-A selection, enzymatic fragmentation, and generation of double-stranded cDNA using a mixture of Oligo (dT) and random priming. The cDNA underwent end repair, ligation of dual-index adaptors, strand selection, and 15 cycles of PCR amplification. We measured purified library concentrations with the Qubit 1X dsDNA HS Assay Kit (Invitrogen Q33231), and libraries were pooled in equimolar amounts based on the Qubit concentration and TapeStation average size and run on MiniSeq for index balancing. The final, purified pool was quantified by qPCR. Raw reads were aligned to the reference genome hg38 using STAR ([Dobin et al., 2013]()). ENSEMBL gene expression was quantified using FeatureCounts ([Liao et al., 2014]()). Normalized and differential expression statistics were computed using edgeR ([Robinson et al., 2010]()), and p values were adjusted for multiple testing using the false discovery rate (FDR) correction of Benjamini and Hochberg. We identified DEGs with q value <0.05 and a log 2 fold change ≥2 between control and AF iPSC-aCMs. We performed unsupervised hierarchical clustering of all DEG using the Euclidean distance and complete linkage method and generated volcano plots using R. Up- and downregulated genes were analyzed separately using the DAVID functional annotation tool against the GO Biological Process (GO) database.

MEA recordings of atrial iPSC-CMs

We used an MEA recording system (MEA2100-Lite-System) to record iPSC-aCMs with the spontaneously beating iPSC-aCMs plated on fibronectin-coated MEA plates. The FPD in both *SCN5A*-E428K and control iPSC-CMs was determined by pacing at 2 Hz. Fridericia's formula was used to standardize the beat rate-associated dispersed FPD:FPDc = FPD/(Beat period)$^{0.3}$. We recorded the extracellular electrograms in DMEM/HEPES at 37°C with the data analyzed using MC-Rack Program (Multichannel Systems). We added ranolazine to the extracellular solution at the desired final concentration.

Patch-clamp recordings of iPSC-aCMs

Patch-clamp measurements were performed in whole-cell configurations using an Axopatch 200B amplifier controlled by pClamp10 software through an Axon Digidata 1440A (Kim et al., 2014). For measurement of sodium currents, external solution contains 50 mM NaCl, 2 mM $CaCl_2$, 100 mM CsCl, 1 mM $MgCl_2$, 10 mM glucose, 10 mM HEPES, and 0.001 mM nifedipine (pH 7.4 with CsOH). Pipette solution contained 135 mM CsCl, 10 mM NaCl, 2 mM $CaCl_2$, 5 mM EGTA, 10 mM HEPES, and 5 mM Mg-ATP (pH 7.2 with CsOH). The current data were analyzed with pCLAMP Software (Pathak et al., 2016). Sodium current densities were calculated according to whole-cell current amplitude and capacitance values obtained from the amplifier following electronic subtraction of the capacitive transients (Hong et al., 2020; Liu et al., 2018). The AP was obtained using the current-clamp mode by injecting stimulus current (2–4 ms, 20–200 pA) at a frequency of 1 Hz (Menon et al., 2019). The current-clamp recordings were recorded in a solution containing 140 mM NaCl, 5.4 mM KCl, 1 mM $MgCl_2$, 10 mM glucose, 2.0 mM $CaCl_2$, and 10 mM HEPES (pH 7.4 with NaOH). The pipette solution contained 120 mM KCl, 1 mM $MgCl_2$, 10 mM HEPES, 2 mM Mg-ATP, and 10 mM EGTA (pH 7.3 with KOH). The AP data were analyzed with pCLAMP Software (Molecular Devices).

Statistics

Data are presented as mean ± standard deviation (SD). For datasets with normal distributions, statistical significance was determined by Student's t test (two-tailed) for two groups or one-way ANOVA for multiple groups with post-hoc Bonferroni corrections.

RNA sequencing data availability

The RNA sequencing data in this article were deposited in the GEO database and the accession number is GSE154084.

SUPPLEMENTAL INFORMATION

Supplemental information can be found online at https://doi.org/10.1016/j.stemcr.2021.04.019.

AUTHOR CONTRIBUTIONS

D.D. and L.H. conceived the project, designed the experiments, analyzed the data, and wrote the manuscript. L.H. performed electrophysiological experiments. M.Z. carried out cell culture, and generated atrial and GC of iPSC lines with the help of H.C. H.C., O.T.L., M.Z., A.S., E.L., and S.-W.Y. performed flow cytometry, cal-

cium handling, qPCR, western blotting, and other molecular analyses. B.C. assisted with obtaining the clinical data. M.M.C., L.F., and J.R. analyzed RNA sequencing data. S.-G.O. and J.C.W. assisted with designing the iPSC differentiation approaches. All authors revised the manuscript.

REFERENCES

Ahern, G.P., Hsu, S.F., Klyachko, V.A., and Jackson, M.B. (2000). Induction of persistent sodium current by exogenous and endogenous nitric oxide. J. Biol. Chem. *275*, 28810–28815.

Antzelevitch, C., Nesterenko, V., Shryock, J.C., Rajamani, S., Song, Y., and Belardinelli, L. (2014). The role of late I Na in development of cardiac arrhythmias. Handb. Exp. Pharmacol. *221*, 137–168.

Argenziano, M., Lambers, E., Hong, L., Sridhar, A., Zhang, M., Chalazan, B., Menon, A., Savio-Galimberti, E., Wu, J.C., Rehman, J., et al. (2018). Electrophysiologic characterization of calcium handling in human induced pluripotent stem cell-derived atrial cardiomyocytes. Stem Cell Reports. *10*, 1867–1878.

Barichello, S., Roberts, J.D., Backx, P., Boyle, P.M., and Laksman, Z. (2018). Personalizing therapy for atrial fibrillation: the role of stem cell and in silico disease models. Cardiovasc. Res. *114*, 931–943.

Benzoni, P., Campostrini, G., Landi, S., Bertini, V., Marchina, E., Iascone, M., Ahlberg, G., Olesen, M.S., Crescini, E., Mora, C., et al. (2020). Human iPSC modelling of a familial form of atrial fibrillation reveals a gain of function of If and ICaL in patient-derived cardiomyocytes. Cardiovasc. Res. *116*, 1147–1160.

Birket, M.J., Ribeiro, M.C., Kosmidis, G., Ward, D., Leitoguinho, A.R., van de Pol, V., Dambrot, C., Devalla, H.D., Davis, R.P., Mastroberardino, P.G., et al. (2015). Contractile defect caused by mutation in MYBPC3 revealed under conditions optimized for human PSC-cardiomyocyte function. Cell Rep. *13*, 733–745.

Chen, Y.H., Xu, S.J., Bendahhou, S., Wang, X.L., Wang, Y., Xu, W.Y., Jin, H.W., Sun, H., Su, X.Y., Zhuang, Q.N., et al. (2003). KCNQ1 gain-of-function mutation in familial atrial fibrillation. Science *299*, 251–254.

Cheng, J., Valdivia, C.R., Vaidyanathan, R., Balijepalli, R.C., Ackerman, M.J., and Makielski, J.C. (2013). Caveolin-3 suppresses late

sodium current by inhibiting nNOS-dependent S-nitrosylation of SCN5A. J. Mol. Cell. Cardiol. *61*, 102–110.

Chugh, S.S., Havmoeller, R., Narayanan, K., Singh, D., Rienstra, M., Benjamin, E.J., Gillum, R.F., Kim, Y.H., McAnulty, J.H., Jr., Zheng, Z.J., et al. (2014). Worldwide epidemiology of atrial fibrillation: a global burden of disease 2010 study. Circulation *129*, 837–847.

Darbar, D., Kannankeril, P.J., Donahue, B.S., Kucera, G., Stubblefield, T., Haines, J.L., George, A.L., Jr., and Roden, D.M. (2008). Cardiac sodium channel (SCN5A) variants associated with atrial fibrillation. Circulation *117*, 1927–1935.

Darbar, D., and Roden, D.M. (2013). Genetic mechanisms of atrial fibrillation: impact on response to treatment. Nat. Rev. Cardiol. *10*, 317–329.

Darghosian, L., Free, M., Li, J., Gebretsadik, T., Bian, A., Shintani, A., McBride, B.F., Solus, J., Milne, G., Crossley, G.H., et al. (2015). Effect of omega-three polyunsaturated fatty acids on inflammation, oxidative stress, and recurrence of atrial fibrillation. Am. J. Cardiol. *115*, 196–201.

Devalla, H.D., Schwach, V., Ford, J.W., Milnes, J.T., El-Haou, S., Jackson, C., Gkatzis, K., Elliott, D.A., Chuva de Sousa Lopes, S.M., Mummery, C.L., et al. (2015). Atrial-like cardiomyocytes from human pluripotent stem cells are a robust preclinical model for assessing atrial-selective pharmacology. EMBO Mol. Med. *7*, 394–410.

Dobin, A., Davis, C.A., Schlesinger, F., Drenkow, J., Zaleski, C., Jha, S., Batut, P., Chaisson, M., and Gingeras, T.R. (2013). STAR: ultrafast universal RNA-seq aligner. Bioinformatics *29*, 15–21.

Enriquez, A., Antzelevitch, C., Bismah, V., and Baranchuk, A. (2016). Atrial fibrillation in inherited cardiac channelopathies: from mechanisms to management. Heart Rhythm *13*, 1878–1884.

Friberg, J., Buch, P., Scharling, H., Gadsbphioll, N., and Jensen, G.B. (2003). Rising rates of hospital admissions for atrial fibrillation. Epidemiology *14*, 666–672.

Gudbjartsson, D.F., Holm, H., Sulem, P., Masson, G., Oddsson, A., Magnusson, O.T., Saemundsdottir, J., Helgadottir, H.T., Helgason, H., Johannsdottir, H., et al. (2017). A frameshift deletion in the sarcomere gene MYL4 causes early-onset familial atrial fibrillation. Eur. Heart J. *38*, 27–34.

Gupta, T., Khera, S., Kolte, D., Aronow, W.S., and Iwai, S. (2015). Antiarrhythmic properties of ranolazine: a review of the current evidence. Int. J. Cardiol. *187*, 66–74.

Hashambhoy, Y.L., Winslow, R.L., and Greenstein, J.L. (2011). CaMKII-dependent activation of late INa contributes to cellular arrhythmia in a model of the cardiac myocyte. Annu Int Conf IEEE Eng Med Biol Soc, 4665–4668.

Heijman, J., Schirmer, I., and Dobrev, D. (2016). The multiple proarrhythmic roles of cardiac calcium-handling abnormalities: triggered activity, conduction abnormalities, beat-to-beat variability, and adverse remodelling. Europace *18*, 1452–1454.

Heijman, J., Voigt, N., Nattel, S., and Dobrev, D. (2012). Calcium handling and atrial fibrillation. Wien Med Wochenschr *162*, 287–291.

Herron, T.J., Rocha, A.M., Campbell, K.F., Ponce-Balbuena, D., Willis, B.C., Guerrero-Serna, G., Liu, Q., Klos, M., Musa, H., Zarzoso, M., et al. (2016). Extracellular matrix-mediated maturation of hu-man pluripotent stem cell-derived cardiac monolayer structure and electrophysiological function. Circ. Arrhythm Electrophysiol. *9*, e003638.

Hong, L., Zhang, M., Sridhar, A., and Darbar, D. (2020). Pathogenic mutations perturb calmodulin regulation of Nav1.8 channel. Biochem. Biophys. Res. Commun. *533*, 168–174.

House, C.D., Vaske, C.J., Schwartz, A.M., Obias, V., Frank, B., Luu, T., Sarvazyan, N., Irby, R., Strausberg, R.L., Hales, T.G., et al. (2010). Voltage-gated Na+ channel SCN5A is a key regulator of a gene transcriptional network that controls colon cancer invasion. Cancer Res *70*, 6957–6967.

Itzhaki, I., Maizels, L., Huber, I., Zwi-Dantsis, L., Caspi, O., Winterstern, A., Feldman, O., Gepstein, A., Arbel, G., Hammerman, H., et al. (2011). Modelling the long QT syndrome with induced pluripotent stem cells. Nature *471*, 225–229.

January, C.T., Wann, L.S., Alpert, J.S., Calkins, H., Cigarroa, J.E., Cleveland, J.C., Jr., Conti, J.B., Ellinor, P.T., Ezekowitz, M.D., Field, M.E., et al. (2014). 2014 AHA/ACC/HRS guideline for the management of patients with atrial fibrillation: a report of the American College of Cardiology/American Heart Association Task Force on Practice Guidelines and the Heart Rhythm Society. J. Am. Coll. Cardiol. *64*, e1–76.

Juretic, N., Urzua, U., Munroe, D.J., Jaimovich, E., and Riveros, N. (2007). Differential gene expression in skeletal muscle cells after membrane depolarization. J Cell Physiol *210*, 819–830.

Kim, I.H., Hevezi, P., Varga, C., Pathak, M.M., Hong, L., Ta, D., Tran, C.T., Zlotnik, A., Soltesz, I., and Tombola, F. (2014). Evidence for functional diversity between the voltage-gated proton channel Hv1 and its closest related protein HVRP1. PLoS One *9*, e105926.

Lee, J.H., Protze, S.I., Laksman, Z., Backx, P.H., and Keller, G.M. (2017). Human pluripotent stem cell-derived atrial and ventricular cardiomyocytes develop from distinct mesoderm populations. Cell Stem Cell *21*, 179–194 e174.

Li, Q., Huang, H., Liu, G., Lam, K., Rutberg, J., Green, M.S., Birnie, D.H., Lemery, R., Chahine, M., and Gollob, M.H. (2009). Gain-of-function mutation of Nav1.5 in atrial fibrillation enhances cellular excitability and lowers the threshold for action potential firing. Biochem. Biophys. Res. Commun. *380*, 132–137.

Liang, P., Sallam, K., Wu, H., Li, Y., Itzhaki, I., Garg, P., Zhang, Y., Vermglinchan, V., Lan, F., Gu, M., et al. (2016). Patient-specific and genome-edited induced pluripotent stem cell-derived cardiomyocytes elucidate single-cell phenotype of Brugada syndrome. J. Am. Coll. Cardiol. *68*, 2086–2096.

Liao, Y., Smyth, G.K., and Shi, W. (2014). featureCounts: an efficient general purpose program for assigning sequence reads to genomic features. Bioinformatics *30*, 923–930.

Lieve, K.V., Verkerk, A.O., Podliesna, S., van der Werf, C., Tanck, M.W., Hofman, N., van Bergen, P.F., Beekman, L., Bezzina, C.R., Wilde, A.A.M., et al. (2017). Gain-of-function mutation in SCN5A causes ventricular arrhythmias and early onset atrial fibrillation. Int. J. Cardiol. *236*, 187–193.

Liu, J., Liu, D., Liu, J.J., Zhao, C., Yao, S., and Hong, L. (2018). Blocking the Nav1.5 channel using eicosapentaenoic acid reduces migration and proliferation of ovarian cancer cells. Int. J. Oncol. *53*, 855–865.

Makielski, J.C. (2016). Late sodium current: A mechanism for angina, heart failure, and arrhythmia. Trends Cardiovasc Med *26*, 115–122.

Menon, A., Hong, L., Savio-Galimberti, E., Sridhar, A., Youn, S.W., Zhang, M., Kor, K., Blair, M., Kupershmidt, S., and Darbar, D. (2019). Electrophysiologic and molecular mechanisms of a frameshift NPPA mutation linked with familial atrial fibrillation. J. Mol. Cell. Cardiol. *132*, 24–35.

Moretti, A., Bellin, M., Welling, A., Jung, C.B., Lam, J.T., Bott-Flugel, L., Dorn, T., Goedel, A., Hohnke, C., Hofmann, F., et al. (2010). Patient-specific induced pluripotent stem-cell models for long-QT syndrome. N. Engl. J. Med. *363*, 1397–1409.

Orr, N., Arnaout, R., Gula, L.J., Spears, D.A., Leong-Sit, P., Li, Q., Tarhuni, W., Reischauer, S., Chauhan, V.S., Borkovich, M., et al. (2016). A mutation in the atrial-specific myosin light chain gene (MYL4) causes familial atrial fibrillation. Nat. Commun. *7*, 11303.

Otway, R., Vandenberg, J.I., Guo, G., Varghese, A., Castro, M.L., Liu, J., Zhao, J., Bursill, J.A., Wyse, K.R., Crotty, H., et al. (2007). Stretch-sensitive KCNQ1 mutation A link between genetic and environmental factors in the pathogenesis of atrial fibrillation? J. Am. Coll. Cardiol. *49*, 578–586.

Pathak, M.M., Tran, T., Hong, L., Joos, B., Morris, C.E., and Tombola, F. (2016). The Hv1 proton channel responds to mechanical stimuli. J. Gen. Physiol. *148*, 405–418.

Peng, W., Li, M., Li, H., Tang, K., Zhuang, J., Zhang, J., Xiao, J., Jiang, H., Li, D., Yu, Y., et al. (2017). Dysfunction of myosin light-chain 4 (MYL4) leads to heritable atrial cardiomyopathy with electrical, contractile, and structural components: evidence from genetically-engineered rats. J. Am. Heart Assoc. *6*, e007030.

Polytarchou, K., and Manolis, A.S. (2015). Ranolazine and its anti-arrhythmic actions. Cardiovasc. Hematol. Agents Med. Chem. *13*, 31–39.

Ritchie, M.D., Rowan, S., Kucera, G., Stubblefield, T., Blair, M., Carter, S., Roden, D.M., and Darbar, D. (2012). Chromosome 4q25 variants are genetic modifiers of rare ion channel mutations associated with familial atrial fibrillation. J. Am. Coll. Cardiol. *60*, 1173–1181.

Robinson, M.D., McCarthy, D.J., and Smyth, G.K. (2010). edgeR: a Bioconductor package for differential expression analysis of digital gene expression data. Bioinformatics *26*, 139–140.

Ronchi, C., Bernardi, J., Mura, M., Stefanello, M., Badone, B., Rocchetti, M., Crotti, L., Brink, P., Schwartz, P.J., Gnecchi, M., et al. (2020). NOS1AP polymorphisms reduce NOS1 activity and interact with prolonged repolarization in arrhythmogenesis. Cardiovasc. Res. *117*, 472–483.

Savio-Galimberti, E., and Darbar, D. (2014). Atrial fibrillation and SCN5A variants. Card Electrophysiol. Clin. *6*, 741–748.

Tobin, M.D., Kahonen, M., Braund, P., Nieminen, T., Hajat, C., Tomaszewski, M., Viik, J., Lehtinen, R., Ng, G.A., Macfarlane, P.W., et al. (2008). Gender and effects of a common genetic variant in the NOS1 regulator NOS1AP on cardiac repolarization in 3761 individuals from two independent populations. Int. J. Epidemiol. *37*, 1132–1141.

Tolon, R.M., Sanchez-Franco, F., Lopez Fernandez, J., Lorenzo, M.J., Vazquez, G.F., and Cacicedo, L. (1996). Regulation of somatostatin gene expression by veratridine-induced depolarization in cultured fetal cerebrocortical cells. Brain Res Mol Brain Res *35*, 103–110.

Wagner, S., Dybkova, N., Rasenack, E.C., Jacobshagen, C., Fabritz, L., Kirchhof, P., Maier, S.K., Zhang, T., Hasenfuss, G., Brown, J.H., et al. (2006). Ca2+/calmodulin-dependent protein kinase II regulates cardiac Na+ channels. J Clin Invest *116*, 3127–3138.

Watanabe, H., Yang, T., Stroud, D.M., Lowe, J.S., Harris, L., Atack, T.C., Wang, D.W., Hipkens, S.B., Leake, B., Hall, L., et al. (2011). Striking in vivo phenotype of a disease-associated human SCN5A mutation producing minimal changes in vitro. Circulation *124*, 1001–1011.

Zimetbaum, P. (2010). In the clinic. Atrial fibrillation. Ann. Intern. Med. *153*, ITC61-15.